J. Plasma Physics (2012), vol. 78, part 6, pp. 663–672. © Cambridge University Press 2012
doi:10.1017/S0022377812000554

Numerical study of collisionless $q = 1$ double tearing instability in a cylindrical plasma

LAI WEI[1], XUEFENG YANG[2], SHU ZHENG[1] and YUE LIU[1]

[1]Key Laboratory of Materials Modification by Beams of the Ministry of Education, School of Physics and Optoelectronic Technology, Dalian University of Technology, Dalian 116024, China (zhengshu@dlut.edu.cn)
[2]School of Mathematical Science, Dalian University of Technology, Dalian 116024, China

(Received 12 March 2012; revised 11 May 2012; accepted 14 May 2012; first published online 3 July 2012)

Abstract. The double tearing mode (DTM) instability with two $q_s = 1$ rational surfaces is investigated by taking into account the collisionless effects, including electron inertia and electron viscosity in a cylindrical geometry. The calculations show that for q-profile with a small distance between two rational surfaces, Δr_s, there exists a broad linear spectrum of collisionless DTMs. The collisionless effects not only can significantly increase the linear growth rate of DTMs but can also enlarge the width of spectrum of unstable modes. For the q-profile with fixed Δr_s and fixed magnetic shears at two rational surfaces, the high-order harmonics with smaller wavelength, such as the $m/n = 2/2$, $3/3$ and $4/4$ modes, can be easily excited to have larger growth rates than the $m/n = 1/1$ mode by 'lifting' the safety factor value between two rational surfaces. The characteristics of eigenmode structures of the most unstable and secondly unstable DTMs with various mode numbers are analyzed in detail and the corresponding collisionless scalings are numerically obtained and verified theoretically based on the previous relevant analytical theories. In addition, the synergetic effects of plasma resistivity, electron inertia and electron viscosity on the linear growth rates of DTMs are analyzed.

1. Introduction

Collisionless effects, such as electron inertia and the Hall effects, play significant roles in accelerating magnetic reconnection during substorms in the Earth magnetosphere and sawtooth oscillations in tokamak experiments (Coppi et al. 1979; Porcelli 1991; Aydemir 1992; Ottaviani and Porcelli 1993; Wang and Bhattacharjee 1993; Kleva et al. 1995; Matsumoto et al. 1999; Birn et al. 2001; Ishizawa et al. 2003; Yamada et al. 2010). Within the framework of the collisionless magnetohydrodynamics (MHD) theory, electron inertia rather than collision resistivity is mainly responsible for tearing magnetic field lines, and the Hall effects may significantly enhance the fast magnetic reconnection rate. Furthermore, the tearing mode mediated by dissipative electron viscosity, which can cause plasma current penetration across equilibrium magnetic flux surfaces, is also important for disruption instability and edge localized mode crashes in magnetic fusion devices (Kaw et al. 1979; Aydemir 1990; Yu 1995; Dong et al. 2003; Xu et al. 2010).

Reversed magnetic shear (RMS) is a favorable configuration for improving confinement in core region by suppressing some micro-instabilities or triggering internal transport barrier (ITB) (Kadomtsev and Pogutse 1967; Rosenbluth and Sloan 1971; Fujita et al. 1997; Dong et al. 2004; Yuh et al. 2011; Wang et al. 2009a, b, 2011). However, the associated non-monotonic safety factor q-profile has a pair of resonant surfaces $k_\parallel = (m/q - n)/R_0 = 0$ with the same rational value $q_s = m/n$, where R_0 is the toroidal radius, and m and n are the poloidal and toroidal mode numbers, respectively. Thus, the mutual interaction of tearing instabilities driven by the equilibrium current at each resonant surface leads to a coupled global-type displacement between two rational surfaces, especially in the case of a small rational surface separation, Δr_s (Bierwage and Yu 2007). The behavior of this coupled tearing instability, which is referred to as double tearing mode (DTM) (Furth et al. 1973; Pritchett et al. 1980; Persson and Dewar 1994; Chang et al. 1996; Yu and Günter 1999; Fredrickson et al. 2000; Ishii et al. 2002; Bierwage et al. 2005; Matsumoto et al. 2005; Wang et al. 2007a, b, 2008; Zhang and Ma 2009; He et al. 2010; Janvier et al. 2011; Zhao et al. 2011), is similar to the $m = 1$ kink tearing mode (KTM). The corresponding tearing instability parameter Δ', approaches infinite near the rational surfaces for both DTMs and KTMs, where Δ' is a characteristic quantity of the free magnetic energy available for the tearing mode growth. The resistivity and collisionless scalings of these large Δ' behavior-tearing modes are quite different from the small Δ' tearing modes with their eigenmode perturbations localized around the rational surface because of finite Δ'. It has been found that the

https://doi.org/10.1017/S0022377812000554 Published online by Cambridge University Press

dependence of growth rates of large Δ' tearing modes (e.g. $m = 1$ KTM and low-m DTM with small Δr_s) on resistivity η, electron inertial skin depth $d_e = c/\omega_{pe}$ and electron viscosity μ_e are $\gamma \sim \eta^{1/3}$, $\sim d_e^1$ and $\sim \mu_e^{1/5}$, respectively, where ω_{pe} is the electron plasma frequency. However, the corresponding scalings are $\sim \eta^{3/5}$, $\sim d_e^3$ and $\sim \mu_e^{1/3}$ for the small Δ' tearing modes with relatively slower growth rates (e.g. $m > 1$ single tearing modes (STMs), the high-m/short wavelength DTMs or the weakly coupled DTMs with large Δr_s) (Furth et al. 1963; Coppi 1964; Rosenbluth et al. 1973; Basu and Coppi 1981; Porcelli 1991; Ottaviani and Porcelli 1995; Ishii et al. 2000; Dong et al. 2003; Bhattacharjee et al. 2005; Bierwage et al. 2005; He et al. 2010; Wang et al. 2011c; Wei et al. 2011).

In high-temperature plasmas, classical resistivity with magnetic Reynolds number $S_{Hp} = \tau_\eta/\tau_{Hp} \sim 10^8 - 10^{12}$ is too low to account for the very fast sawtooth relaxation, where τ_η and τ_{Hp} are the resistive diffusion time and poloidal Alfvén time, respectively. It is necessary to take into account the collisionless terms for explaining the short time scale, since the collisionless terms, such as electron inertial and electron viscosity, can greatly enhance the growth rate, particularly for the large Δ' tearing modes. Thus, the roles of collisionless effects on the strongly coupled tearing modes and the resultant off-axis sawtooth crash should also be considered.

In order to study the roles of collisionless effects on tearing modes, we numerically investigate the $q = 1$ DTM instabilities in RMS configuration by taking into account electron inertia and electron viscosity. Particular attention is paid to the characteristics of the eigenmode structures of the most unstable and secondly unstable collisionless $q = 1$ DTMs with different Δr_s. The synergetic effects of resistivity, electron inertia and electron viscosity on linear growth rates with various mode numbers are also discussed.

The remainder of this paper is organized as follows. The modeling equations and equilibrium configurations are described in Sec. 2. In Sec. 3, characteristics of the broad spectrum and the eigenmode structures with various mode numbers are analyzed. In Sec. 4, synergetic effects of η, d_e and μ_e on the growth rate are discussed. Finally, the discussion and conclusions are presented in Sec. 5.

2. Modeling equations and equilibrium configurations

In the high-aspect-ratio and zero β limits, where β is the ratio of thermal to magnetic pressure, a set of reduced collisionless incompressible MHD equations in a cylindrical geometry is employed (Strauss 1976; Hazeltine et al. 1985; Biskamp 1993; Ishii et al. 2002; Bierwage et al. 2005). Thus, the magnetic field and the velocity can be expressed by magnetic flux and stream function as $\mathbf{B} = B_0\hat{\zeta} + \nabla\psi \times \hat{\zeta}$ and $\mathbf{v} = -\nabla\phi \times \hat{\zeta}$, where $\hat{\zeta} \equiv -\hat{z}/R_0 q(a)$ is a unit vector in axial direction.

In the collisionless MHD equations, the electric field $\mathbf{E}$ is given by the generalized Ohm's law with electron inertia and electron viscosity terms included:

$$\mathbf{E} = -\mathbf{v} \times \mathbf{B} + \eta\mathbf{J} + \frac{m_e}{ne^2}\frac{d\mathbf{J}}{dt} - \frac{m_e\mu_e}{ne^2}\nabla^2\mathbf{J}, \qquad (1)$$

where $\mathbf{v}$ is the plasma flow velocity, $\mathbf{J}$ is the current density, n is the electron density and m_e is the electron mass.

From (1), the normalized 2-field governing equations can be expressed as follows (Ishii et al. 2002; Bierwage et al. 2005; He et al. 2010; Wang et al. 2011c; Wei et al. 2011):

$$\frac{\partial F}{\partial t} = [F, \phi] - \frac{\partial \phi}{\partial \zeta} + S_{Hp}^{-1}\nabla_\perp^2 F - R^{-1}\nabla_\perp^2 j_\zeta, \qquad (2)$$

$$\frac{\partial U}{\partial t} = [U, \phi] + [j_\zeta, \psi] + \frac{\partial j_\zeta}{\partial \zeta} + Re_{Hp}^{-1}\nabla_\perp^2 U, \qquad (3)$$

here $j_\zeta = -\nabla^2\psi$ is the axial current density, $F = \psi + d_e^2 j_\zeta$ is the generalized flux function and $U = \nabla^2\phi$ denotes the corresponding vorticity. In the cylindrical system, the Poisson bracket and the Laplacian operator $\nabla_\perp^2$ are defined, respectively, as follows:

$$[f, g] = \frac{1}{r}\left(\frac{\partial f}{\partial r}\frac{\partial g}{\partial \theta} - \frac{\partial g}{\partial r}\frac{\partial f}{\partial \theta}\right) \quad \text{and} \quad \nabla_\perp^2 = \frac{1}{r}\left(\frac{\partial}{\partial r} r \frac{\partial}{\partial r}\right) + \frac{1}{r^2}\frac{\partial^2}{\partial \theta^2}.$$

$Re_{Hp} = \tau_{\mu_i}/\tau_{Hp}$ and $R = \tau_{\mu_e}/\tau_{Hp}$ are ion and electron dynamic Reynolds numbers, respectively, which measure the strength of the viscous diffusions of vorticity and plasma current. In (2) and (3), the time and length are normalized by the poloidal Alfven time $\tau_{Hp} = \sqrt{\rho}a/B_\theta(a)$ and the plasma minor radius a, where $B_\theta(a)$ is the poloidal magnetic field on the plasma surface.

A static equilibrium state is assumed with $\bar{\phi}_{eq} = \bar{U}_{eq} = 0$, and each field perturbation is Fourier transformed as

$$\tilde{f}(r, \vartheta, \xi, t) = \tfrac{1}{2}\sum_{m,n} \tilde{f}_{m,n}(r, t) e^{i(m\theta - n\xi)} + c.c. \qquad (4)$$

Then using the exponential form of each time-dependent radial perturbation with $\tilde{f}(r, t) = \tilde{f}(r)\exp(\lambda t)$, where $\lambda = \gamma + i\omega$ is a complex number with γ being the growth rate and ω being the mode frequency, the individual Fourier component of the linearized equations (2) and (3) with the relations of $q^{-1}(r) = -\frac{1}{r}\frac{d}{dr}\bar{\psi}_{eq}(r)$ and $j_\zeta(r) = \frac{1}{r}\frac{d}{dr}\frac{r^2}{q(r)}$ can be written as follows:

$$\left[\lambda\left(\frac{1}{\nabla_\perp^2} - d_e^2\right) - S_{Hp}^{-1} + R^{-1}\nabla_\perp^2\right]\nabla_\perp^2\tilde{\psi} = \frac{id_e^2}{qr^2}\left[m\left(s^2 - 2s - r\frac{ds}{dr}\right) + (nq - m)\frac{r^2}{d_e^2}\right]\tilde{\phi}, \qquad (5)$$

https://doi.org/10.1017/S0022377812000554 Published online by Cambridge University Press

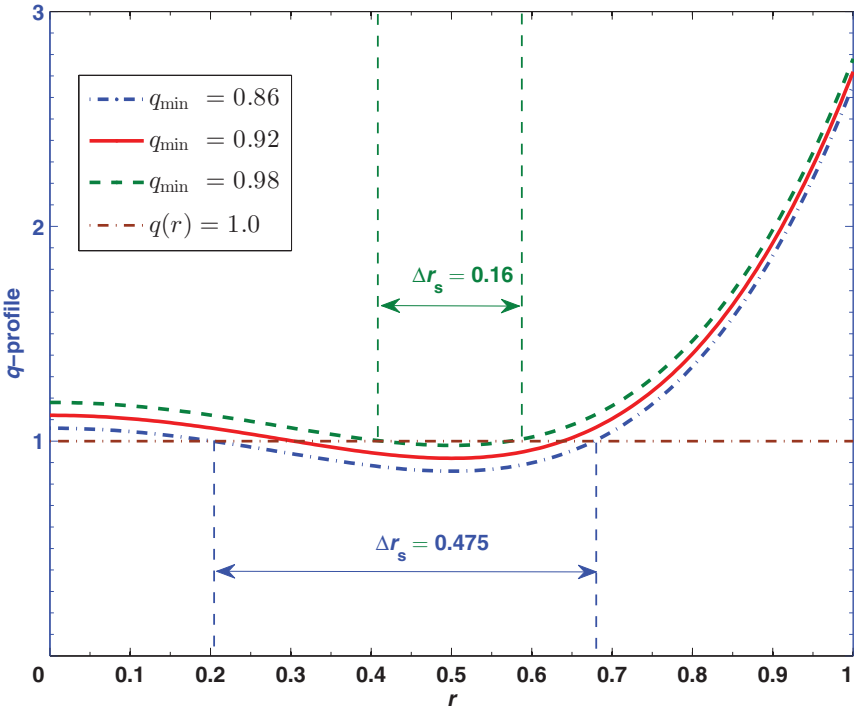


Figure 1. (Colour online). The safety factor q-profiles with two resonance surfaces. The inter-resonance separations are $\Delta r_s = 0.475$, 0.335 and 0.16.

$$\left(\lambda - Re_{Hp}^{-1}\nabla_\perp^2\right)\nabla_\perp^2\tilde{\phi} = \frac{i}{qr^2}\left[m\left(s(s-2) - r\frac{ds}{dr}\right) + (nq-m)\,r^2\nabla_\perp^2\right]\tilde{\psi}, \tag{6}$$

with $s = \frac{r}{q(r)}\frac{dq(r)}{dr}$ being the magnetic shear.

The modeling formula of the non-monotonic q with weak RMS in the center region is given by (Hastie et al. 1987; Bierwage et al. 2005)

$$q(r) = \left(q_{\min} + 0.2[1 + (r/r_0)^2]^2\right)\cdot\left(1 + f_1\cdot e^{-\left(\frac{r-r_0}{d_0}\right)^2}\right), \tag{7}$$

with $q_{\min}$ being the minimum value of the safety factor located at r_0 for $f_1 = 0$. The parameters f_1 and d_0 are used to change the local value of the safety factor near r_0.

Then (5) and (6) can be solved by an eigenvalue problem (EVP) solver for each individual Fourier component $\{m, n\}$ with an ideally conducting wall condition on the boundary (Ishii et al. 2002; Bierwage et al. 2005; He et al. 2010).

3. The broad unstable spectrum and the eigenmode structures

In this section, the dependence of fast linear growth rate on the poloidal mode number m with various parameter values of Δr_s, S_{Hp}, d_e and R is studied in detail. The corresponding eigenmode structures for the most unstable and secondly unstable modes with various m numbers are compared. Furthermore, the benchmark of numerical scalings for different m modes is tested by previous relevant analytical theories based on the similarity of physical characteristics of the same Δ' categories mentioned above.

3.1. The unstable spectrum of DTMs with various Δr_s, S_{Hp}, d_e and R values

As shown in Fig. 1, three q-profiles with various $\Delta r_s = |r_{s1} - r_{s2}|$ are considered first in this work, where $r_{si}\,(i = 1, 2)$ are the radial locations of each resonant surface. The q-profiles are given by (7) with $f_1 = 0$ and $q_{\min} = 0.86$, 0.92 and 0.98. The dispersion relations for different Δr_s with $S_{Hp} = 10^6$, $d_e = 0.005$ and $R = 10^{10}$ are presented in Fig. 2(a). Qualitatively similar to the counterpart in the resistive DTMs, the higher-m mode rather than the $m = 1$ mode is most unstable for small Δr_s case (e.g. the $m = 4$ mode is a dominantly unstable mode in the case of $\Delta r_s = 0.16$). The width of unstable spectrum also increases with decreasing Δr_s. It should be pointed out that there are two unstable eigenmodes for small Δr_s. Hereafter, $M^2$and M^1 denote the most unstable and secondly unstable eigenmodes, respectively. The eigenmode structures for each unstable mode will be discussed later.

Figure 2(b) gives the spectra of unstable DTMs with various S_{Hp}, d_e and R for $\Delta r_s = 0.16$. It is illustrated that both electron inertia and electron viscosity can further enlarge the spectrum width by destabilizing each harmonic component of the unstable modes. This fast growth of the higher-m mode in the linear phase of collisionless $q = 1$ DTMs with electron inertia term

https://doi.org/10.1017/S0022377812000554 Published online by Cambridge University Press

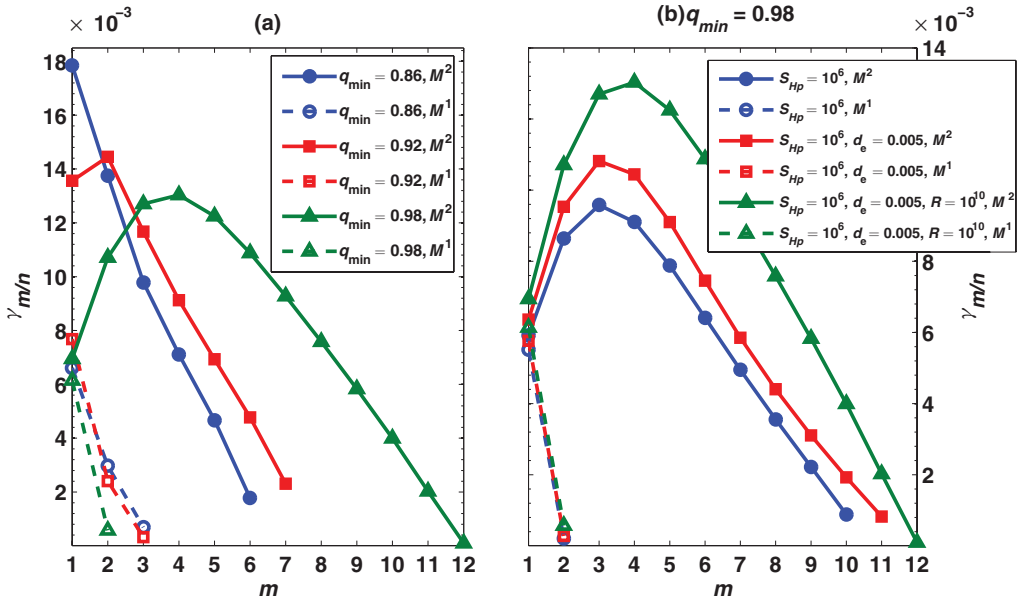


Figure 2. (Colour online). (a) The dispersion relations of $q = 1$ DTMs with $S_{Hp} = 10^6$, $d_e = 0.005$ and $R = 10^{10}$ for different inter-resonance separations Δr_s. (b) The dispersion relations of $q = 1$ DTMs with various S_{Hp}, d_e and R for $\Delta r_s = 0.16$.

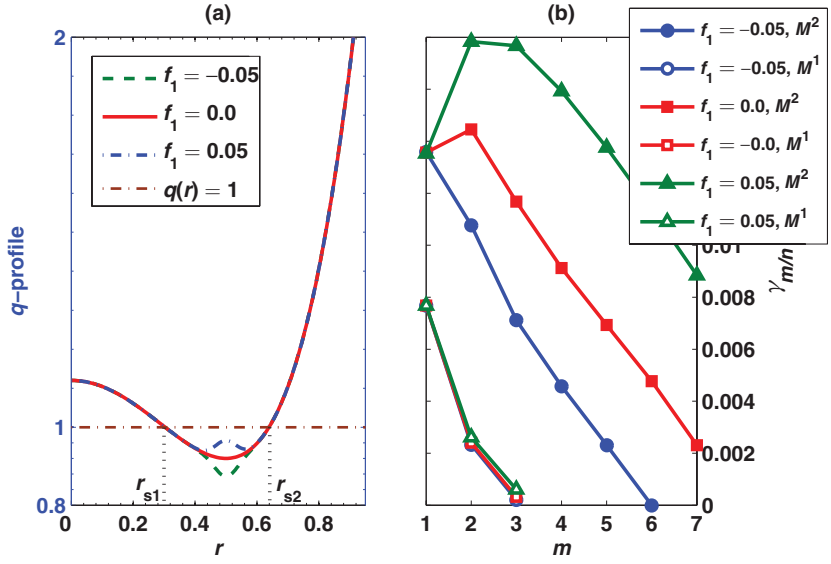


Figure 3. (Colour online). (a) A set of safety factor q-profiles with different safety factor values between two rational surfaces $q(r_{s1} \leqslant r \leqslant r_{s2})$. (b) The dispersion relations of $q = 1$ tearing modes with different $q(r_{s1} \leqslant r \leqslant r_{s2})$.

and electron viscosity also implies that the high-order harmonic $q = 1$ mode, such as $m/n = 2/2$ and $3/3$ modes or even $m/n = 4/4$, should play important roles in the off-axis sawtooth crashes.

3.2. *Effect of the safety factor value between two rational surfaces on the unstable spectrum of DTMs*

It is found in Sec. 3.1 that the high-order harmonic modes are easily excited in the case of a small rational surface separation Δr_s. However, for the q-profile used in Sec. 3.1, not only the inter-surface distance Δr_s of q-profiles but also the safety factor values between two rational surfaces $q(r_{s1} \leqslant r \leqslant r_{s2})$ are different. In order to study the effect of q value between two rational surfaces on the unstable spectrum of DTMs, the modified q-profiles, as shown in Fig. 3(a), are employed in this section. These q-profiles have the same inter-surface distance, Δr_s, and the same magnetic shears at two rational surfaces. The spectra of the growth rate $\gamma_{m/n}$ of various q-profiles are plotted in Fig. 3(b). It is found that the $m = 1$ mode is the most unstable mode for the q-profile with smaller $q(r_{s1} \leqslant r \leqslant r_{s2})$. As $q(r_{s1} \leqslant r \leqslant r_{s2})$ increases, the most unstable mode m_{peak} gradually changes from $m = 1$ to the higher harmonics of $m_{peak} = 2$. Especially, for the q-profile with $q(r_{s1} \leqslant r \leqslant r_{s2}) \to 1$, the high-order harmonics, such as the $m/n = 2/2$, $3/3$ and $4/4$ modes, are excited to a level with higher growth rate than the $m = 1$ mode. Thus, we can get that even for the q-profiles

https://doi.org/10.1017/S0022377812000554 Published online by Cambridge University Press

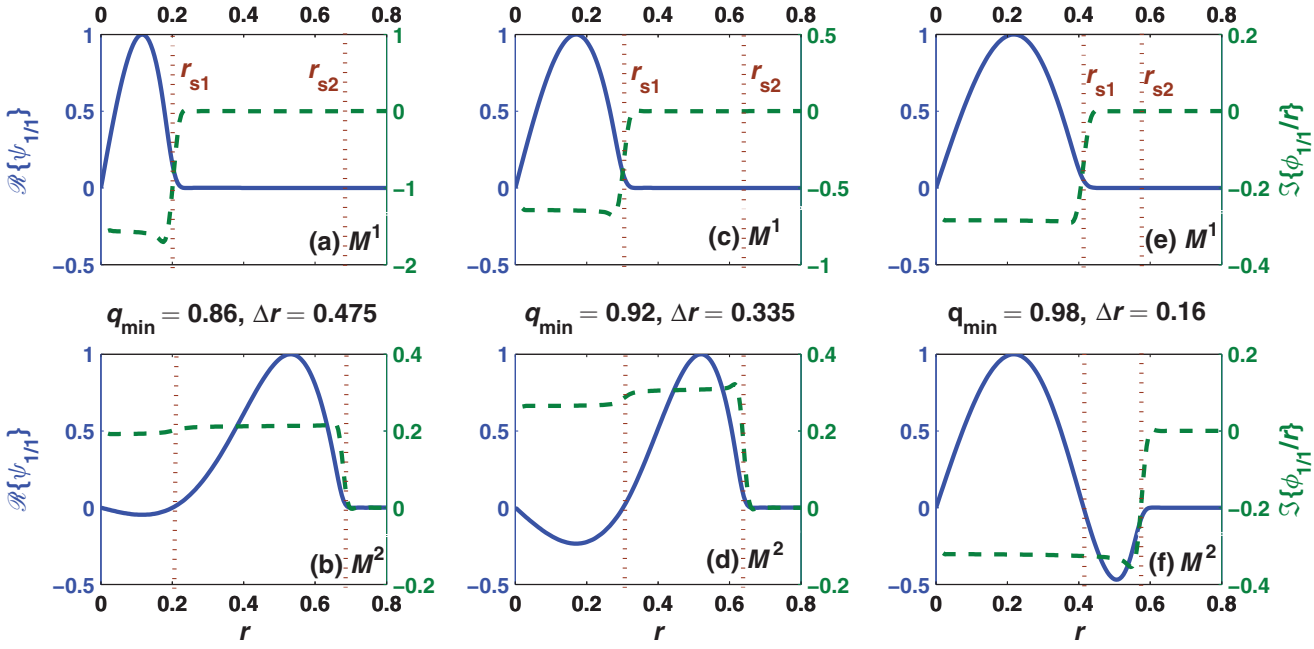


Figure 4. (Colour online). Eigenmode structures of $q = 1$ DTMs with poloidal mode number $m = 1$. The M^1 and M^2 modes for $\Delta r_s = 0.475$ are shown in (a) and (b), for $\Delta r_s = 0.335$ are shown in (c) and (d), for $\Delta r_s = 0.16$ are shown in (e) and (f). The structures of M^1 extends to the inner resonance surface r_{s1}, and M^2 to the outer resonance surface r_{s2}. The blue and the dash green lines represent, respectively, the magnetic flux perturbation $\tilde{\psi}$ and corresponding potential perturbation $\tilde{\phi}/r$.

with fixed Δr_s, the high-order harmonic modes can be easily excited by 'lifting' the q value between two rational surfaces.

3.3. *The unstable mode structures of DTMs with small* Δr_s value

Two forms of $m = 1$ eigenmodes with growth rates $\gamma_{M1} < \gamma_{M2}$ for different q-profiles with various Δr_s are shown in Fig. 4. The rigid global displacements of M^1 modes located in the inner rational surface $0 < r < r_{s1}$ for all three Δr_s cases are shown in Figs. 4(a), (c) and 4(e) with green dashed lines. The characterization of the M^1 mode is the same as $m = 1$ internal resistive KTM. For the M^2 mode, sharp displacements are extended to the outer rational surface $0 < r < r_{s2}$. Interestingly, it is found that the radial profiles of magnetic perturbations have a pair of anti-bumps in the regions of $0 < r < r_{s1}$ and $r_{s1} < r < r_{s2}$, as shown in Figs. 4(b), (d) and (f) with blue lines. Such magnetic perturbations between two rational surfaces shared the same characteristics as the mode structure of the coupled tearing mode (Pritchett et al. 1980).

For the $m = 2$ mode, two forms of mode structures with growth rates $\gamma_{M1} < \gamma_{M2}$ for various Δr_s are shown in Fig. 5. For the M^1 mode with smaller growth rate, it is found that only an STM structure is located on the inner rational surface r_{s1} for the large $\Delta r_s = 0.475$ in Fig. 5(a) or two STMs with weak coupling are located on the two rational surfaces for the small $\Delta r_s = 0.16$ case in Fig. 5(e). On the other hand, for M^2 mode with larger growth rate, the typically coupled DTM structure is located in the inter-rational surface region $r_{s1} < r < r_{s2}$, especially for the small Δr_s case, as illustrated in Fig. 5(f).

In the small $\Delta r_s = 0.16$ case, the high-order harmonic modes are only unstable for the M^2 modes with typical coupled DTM structures. The mode structures for $m = 3, 6, 9, 12$ are shown in Fig. 6. The coupling between two rational surfaces gradually becomes weaker with increasing mode number m, since the tearing instability on each rational surface becomes less unstable with increasing m (Furth et al. 1973). It should be mentioned that the off-axis collapse and the MHD turbulence may be formed quickly in the annular region for the q-profile with small Δr_s because the mode structures of the dominantly unstable high-m modes in the broad spectrum are mainly in the region $r_{s1} < r < r_{s2}$. Such mode structures are quite different from the large Δr_s case, in which the $m = 1$ mode with internal kink structure in the region $0 < r < r_{s2}$ is dominantly unstable.

3.4. *Verification of numerical scalings with various* m values

The η-, d_e- and R-scalings with various mode numbers for $\Delta r_s = 0.16$ are verified by the previous relevant analytical theories based on large Δ' or small Δ' categories. As shown in Fig. 7, the resistive scaling property of DTMs, $\gamma_m \sim \eta^{\alpha_\eta}(S_{Hp}^{-\alpha_\eta})$, is firstly checked by neglecting electron inertia and electron viscosity effects ($d_e \simeq R^{-1} \simeq 0$). In a very large resistivity (or small S_{Hp}) regime, γ_m is increasing with S_{Hp} and the scaling is $\gamma_m \sim S_{Hp}^1(\alpha_\eta = -1)$. However, in a small resistivity (large S_{Hp}) regime, which is of interest for high-temperature plasmas, the scaling is $\sim S_{Hp}^{-1/3}$ for the large Δ' tearing mode (such as M^1 and M^2 of the $m = 1$ mode, as well as M^2 of the low-m mode with coupled mode structure), while the

https://doi.org/10.1017/S0022377812000554 Published online by Cambridge University Press

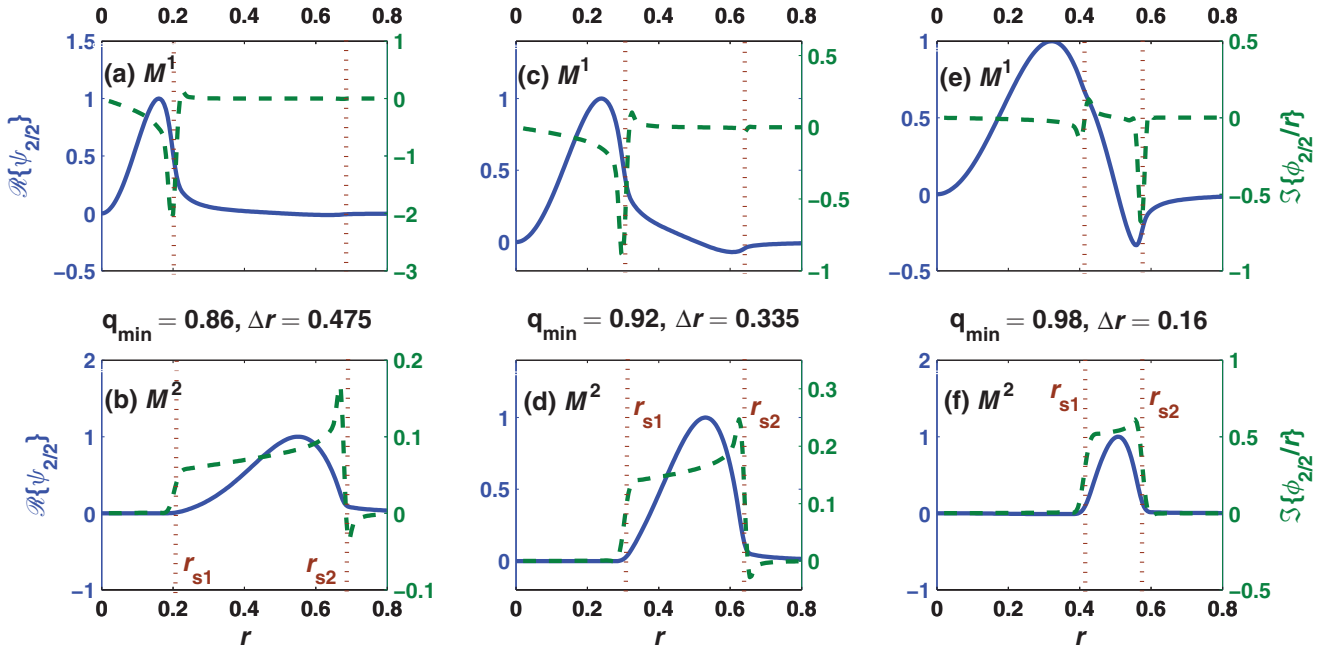


Figure 5. (Colour online). Eigenmode structures of $q = 1$ DTMs with poloidal mode number $m = 2$ for different Δr_s.

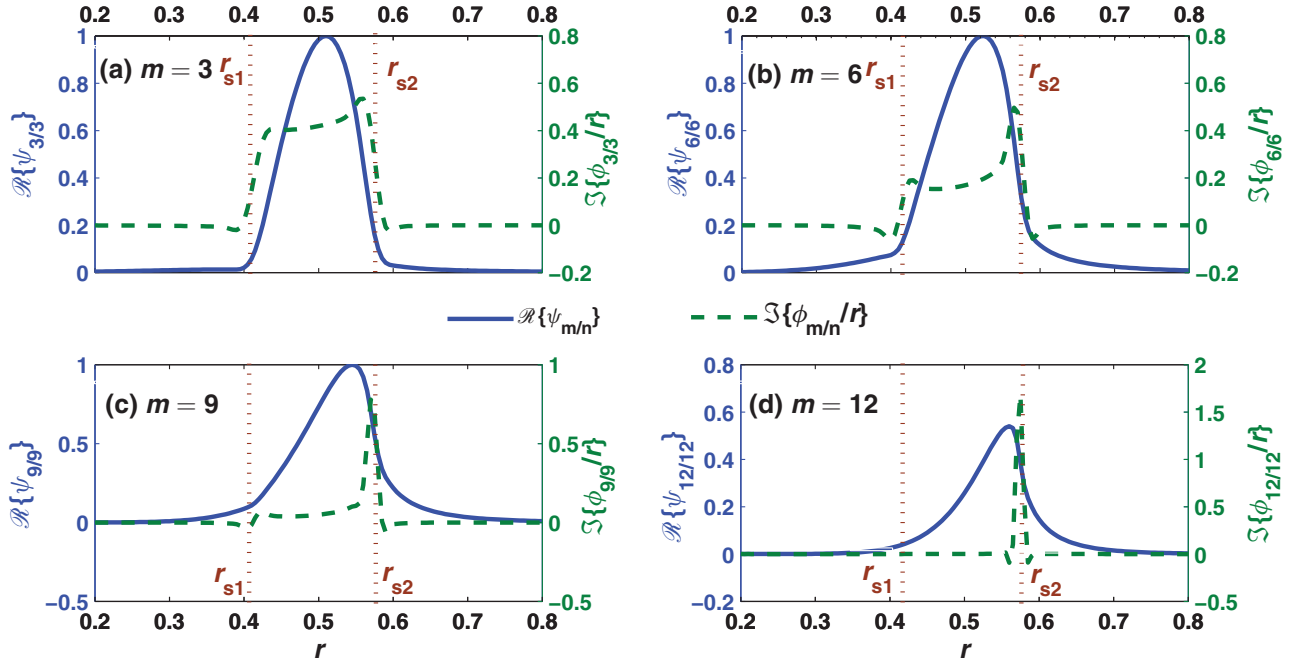


Figure 6. (Colour online). Eigenmode structures of $q = 1$ DTMs with poloidal mode number $m = 3, 6, 9, 12$ for $\Delta r_s = 0.16$.

scaling is $\sim S_{Hp}^{-3/5}$ for the small Δ' tearing mode (such as M^1 of the $m = 2$ mode with STM structures and M^2 of the high-m modes with finite Δ').

The d_e- and R-scalings are shown in Figs. 8 and 9, respectively. Consistent with previous relevant analytical theories (Coppi 1964; Basu and Coppi 1981; Porcelli 1991; Ottaviani and Porcelli 1995; Dong et al. 2003; Bhattacharjee et al. 2005), for the large Δ' tearing mode, the scalings on d_e and R are $\sim d_e^1$ and $\sim R^{-1/5}$, respectively. On the other hand, for the small Δ' tearing mode, the scalings on d_e and R are $\sim d_e^3$ and $\sim R^{-1/3}$, respectively.

The numerical scalings presented above focus only on one of S_{Hp}-, d_e- and R-scalings individually with the other two parameters neglected.

4. Synergetic effects of S_{Hp}, d_e and R

In this section, we consider in detail the synergetic effects of S_{Hp}, d_e and R on the most unstable mode (e.g. the $m = 3$ harmonic for $\Delta r_s = 0.16$ with $S_{Hp} = 10^6$ and $d_e = 0.005$). As shown in Fig. 10(a), the resistivity effect is dominant in very high resistivity regime ($S_{Hp} \leqslant 10^6$), whereas the electron inertia or/and the electron viscosity

https://doi.org/10.1017/S0022377812000554 Published online by Cambridge University Press

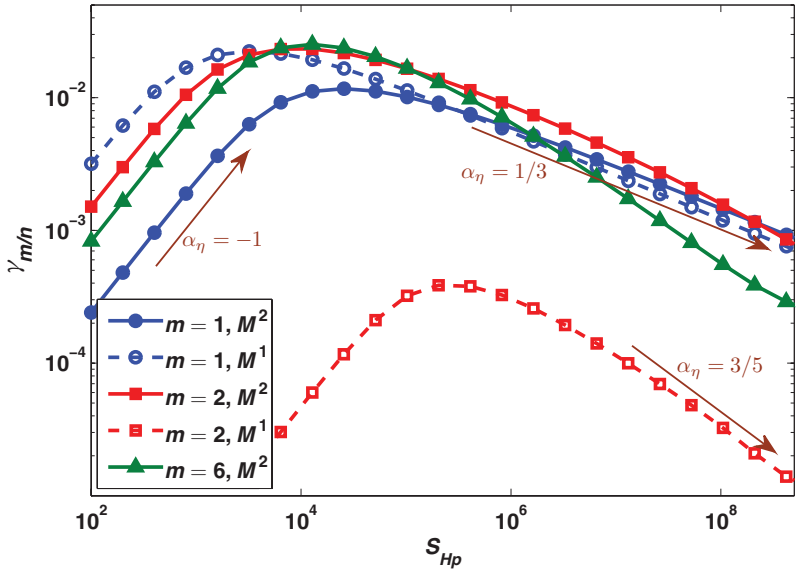


Figure 7. (Colour online). The linear growth rate γ vs. S_{Hp} for different modes. The arrow lines represent the scaling laws $\gamma \sim S_{Hp}^{1}$, $\gamma \sim S_{Hp}^{-3/5}$, and $\gamma \sim S_{Hp}^{-1/3}$, respectively. These results were obtained by setting $d_e \simeq R^{-1} \simeq 0$.

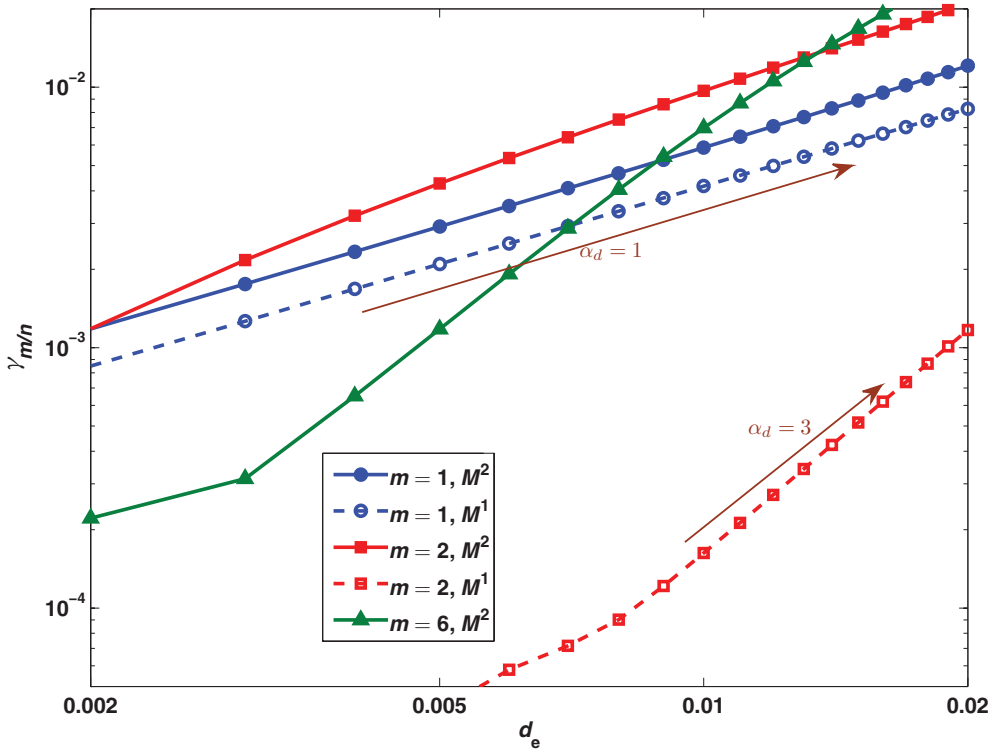


Figure 8. (Colour online). The linear growth rate γ vs. d_e for different modes. The arrow lines represent the scaling laws $\gamma \sim d_e^1$ and $\gamma \sim d_e^3$, respectively. These results were obtained by setting $S_{Hp}^{-1} \simeq R^{-1} \simeq 0$.

instead play a dominant role in accelerating the growth of the mode in the low resistivity regime ($S_{Hp} \geqslant 10^8$), which is of interest for high-temperature plasmas.

The dependence of growth rate on electron viscosity with $d_e = 0.0$ and 0.005 is shown in Fig. 10(b). The synergy regime of electron inertia and electron viscosity for $d_e = 0.005$ is located in the region $10^{10} \leqslant R \leqslant 10^{14}$. For $R < 10^{10}$, the electron viscosity effect is dominant because $\gamma(S_{Hp}^{-1} = 0, R < 10^{10}, d_e = 0) \gg \gamma\ (S_{Hp}^{-1} = 0, R^{-1} = 0,\ d_e = 0.005)$.

Also, it can be found from Figs. 10(a) and (b) that with increasing electron viscosity R^{-1} from 10^{-14} to 10^{-10} for fixed $d_e = 0.005$, the mode transfers from the electron inertia-dominated regime (green diamond line) to the electron viscosity-dominated regime (pink star line) for $S_{Hp} \geqslant 10^8$. Furthermore, for $R^{-1} = 10^{12}$(cyan

https://doi.org/10.1017/S0022377812000554 Published online by Cambridge University Press

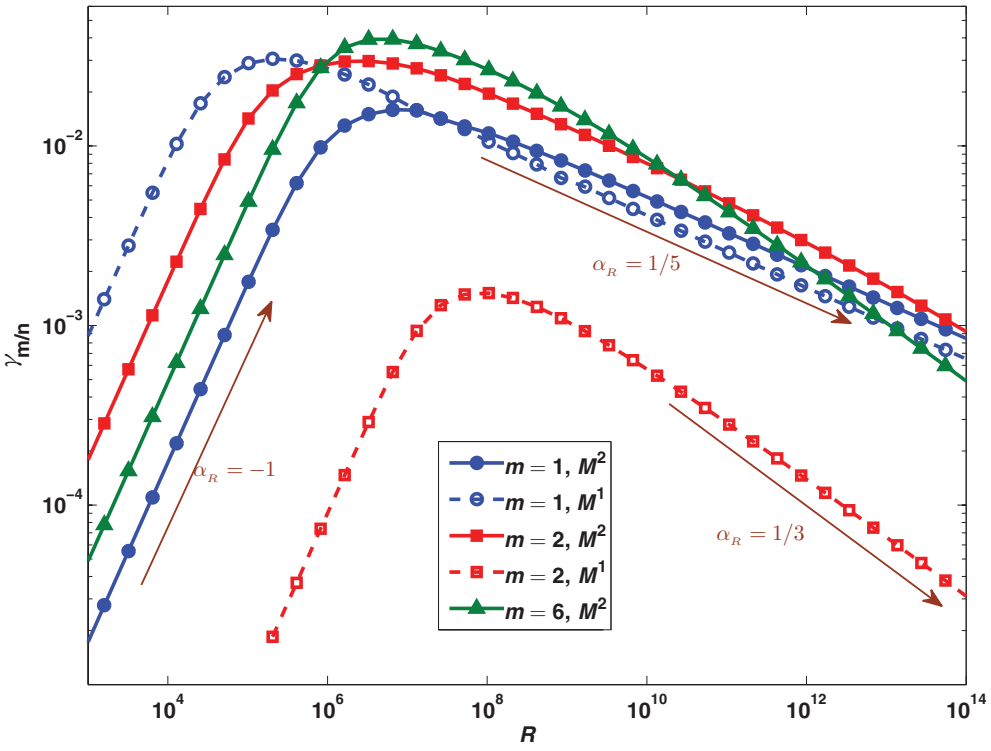


Figure 9. (Colour online). The linear growth rate γ vs. R for different modes. The arrow lines represent the scaling laws $\gamma \sim R^{-1}$, $\gamma \sim R^{-1/3}$ and $\gamma \sim R^{-1/5}$, respectively. These results were obtained by setting $S_{Hp}^{-1} \simeq d_e \simeq 0$.

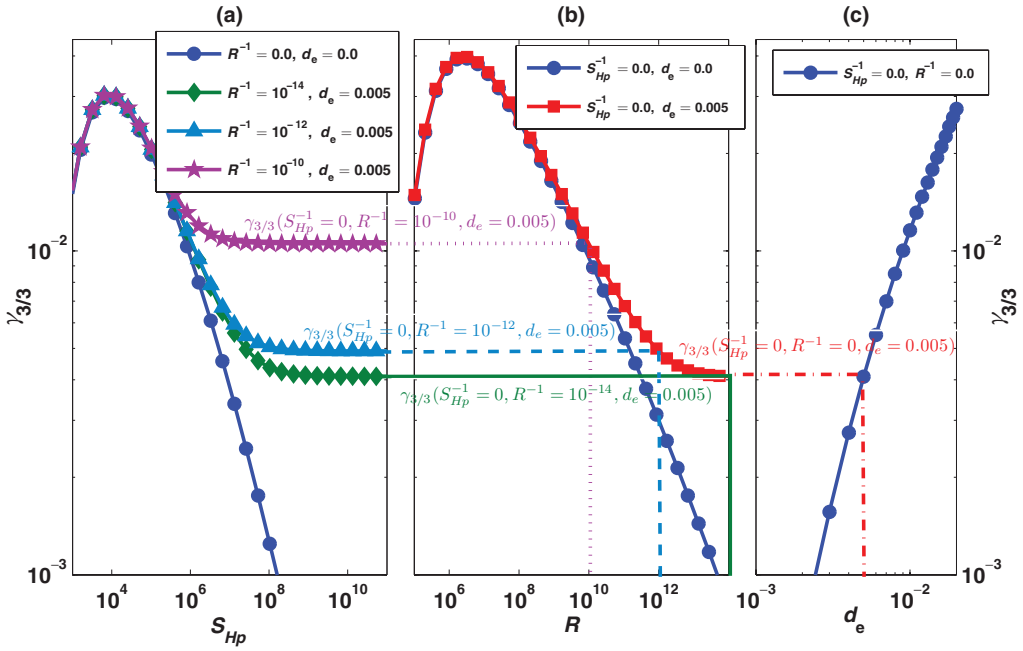


Figure 10. (Colour online) The synergetic effects of S_{Hp}, d_e and R on the $q = 1$ DTM with $\Delta r_s = 0.061$ for poloidal mode number $m = 3$. (a) Dependence of growth rate on S_{Hp} with $d_e = 0.005$ and various R values. (b) Dependence of growth rate on R with $S_{Hp}^{-1} = 0.0$ and various d_e values. (c) Dependence of growth rate on d_e with $S_{Hp}^{-1} = 0.0$ and $R^{-1} = 0.0$.

triangle line), the mode is located in the synergy regime of d_e and R with the linear growth rate being equal to $\gamma(S_{Hp}^{-1} = 0,\ R^{-1} = 10^{-12},\ d_e = 0.05)$.

5. Conclusions

In this paper, the characteristics of the $q = 1$ DTMs with varying distances between two rational surfaces and various mode numbers are investigated within the framework of reduced collisionless MHD model by taking into account the effects of electron inertia and electron viscosity. The detailed properties of the eigenmode structures of the most unstable and secondly unstable DTMs are discussed and the corresponding collisionless scalings are obtained and tested by the

https://doi.org/10.1017/S0022377812000554 Published online by Cambridge University Press

previous relevant analytical theories based on Δ' categories.

It is found that the collisionless effects of electron inertia and electron viscosity play significant roles in increasing the linear growth rate of DTMs and enlarging the width of the spectrum of unstable modes, especially for the small Δr_s case. For q-profile with fixed Δr_s, the high-order harmonic modes can be easily excited by 'lifting' the safety factor value between two rational surfaces. The appearance of the dominant high-order harmonics may be applied to explain some experimental observations, in which the $m/n = 2/2$ and $3/3$ modes were excited before sawtooth crashes (Sun et al. 2009; Papp et al. 2011). Finally, the synergetic effects of resistivity, electron inertia and electron viscosity on the dominant high-m mode are analyzed in detail.

The linear results presented in this work are obtained in a cylindrical geometry by neglecting the toroidal mode coupling effect which may play an important role in the 'infernal' mode for a weak magnetic shear configuration in core plasmas (Charlton et al. 1988, 1989; Nave and Wesson 1988; Ganesh and Vaclavik 2005; Chapman et al. 2010). Moreover, the plasma mean $\mathbf{E} \times \mathbf{B}$ flow and diamagnetic flow, which also have an effect on tearing modes, are not considered in this work (Chen and Morrison 1990; Ofman et al. 1991; Persson 1991; Ofman 1992; Shen and Liu 1998; Bierwage et al. 2007; Ishii et al. 2009; Halpern et al. 2011; Wang et al. 2011a, b, 2012; Wei and Wang 2011). The investigation of the linear and nonlinear drift DTMs, including the toroidal effect, is in progress.

Acknowledgments

This work is supported by NMCSFP Grant Nos. 2011GB107000 and 2010GB106002, NSFC Grant Nos. 11005015 and 10935004, NBRPC with Grant Nos. 2008CB787103 and 2009GB105004, NCET and FRFCU (DUT12ZD201). The simulation is supported by the High Performance Computing Department of Network and Information Center, Dalian University of Technology.

References

Aydemir, A. Y. 1990 *Phys. Fluids* B **2**, 2135.

Aydemir, A. Y. 1992 *Phys. Fluids* B **4**, 3469.

Basu, B. and Coppi, B. 1981 *Phys. Fluids* **24**, 465.

Bhattacharjee, A., Germaschewski, K. and Ng, C. S. 2005 *Phys. Plasmas* **12**, 042305.

Bierwage, A., Benkadda, S., Hamaguchi, S. and Wakatani, M. 2005 *Phys. Plasmas* **12**, 082504.

Bierwage, A., Hamaguchi, S., Wakatani, M. Benkadda, S. and Leoncini, X. 2005 *Phys. Rev. Lett.* **94**, 065001.

Bierwage, A. and Yu, Q. 2007 *Plasma Phys. Control. Fusion* **49**, 675.

Bierwage, A., Yu, Q. and Günter, S. 2007 *Phys. Plasmas* **14**, 010704.

Birn, J., Drake, J. F., Shay, M. A., Rogers, B. N., Denton, R. E., Hesse, M., Kuznetsova, M., Ma, Z. W., Bhattacharjee, A., Otto, A. et al. 2001 *J. Geophys. Res.* **106**, 3751.

Biskamp, D. 1993 *Nonlinear Magnetohydrodynamics*. Cambridge, UK: Cambridge University Press.

Chang, Z., Park, W., Fredrickson, E. D., Batha, S. H., Bell, M. G., Bell, R., Budny, R. V., Bush, C. E., Janos, A., Levinton, F. M. et al. 1996 *Phys. Rev. Lett.* **77**, 3553.

Chapman, I. T., Hua, M. D., Pinches, S. D., Akers, R. J., Field, A. R., Graves, J. P., Hastie, R. J., Michael, C. A. and the MAST Team 2010 *Nucl. Fusion* **50**, 045007.

Charlton, L. A., Carreras, B. A., Holmes, J. A. and Lynch, V. E. 1988 P*hys. Fluids* **31**, 347.

Charlton, L. A., Hastie, R. J. and Hender, T. C. 1989 *Phys. Fluids* B **1**, 798.

Chen, X. L. and Morrison, P. J. 1990 *Phys. Fluids* B **2**, 495.

Coppi, B. 1964 *Phys. Lett.* **11**, 226.

Coppi, B., Mark, J. W.-K., Sugiyama, L. and Bertin, G. 1979 *Phys. Rev. Lett.* **42**, 1058.

Dong, J. Q., Mahajan, S. M. and Horton, W. 2003 *Phys. Plasmas* **10**, 3151.

Dong, J. Q., Mou, Z. Z., Long, Y. X. and Mahajan, S. M. 2004 *Phys. Plasmas* **11**, 5673.

Fredrickson, E., Bell, M., Budny, R. V. and Synakowski, E. 2000 *Phys. Plasmas* **7**, 4112.

Fujita, T., Ide, S., Shirai, H., Kikuchi, M., Naito, O., Koide, Y., Takeji, S., Kubo, H. and Ishida, S. 1997 *Phys. Rev. Lett.* **78**, 2377.

Furth, H. P., Killeen, J. and Rosenbluth, M. N. 1963 *Phys. Fluids* **6**, 459.

Furth, H. P., Rutherford, P. H. and Selberg, H. 1973 *Phys. Fluids* **16**, 1054.

Ganesh, R. and Vaclavik, J. 2005 *Phys. Rev. Lett.* **94**, 145002.

Halpern, F. D., Lütjens, H. and Luciani, J.-F. 2011 *Phys. Plasmas* **18**, 102501.

Hastie, R. J., Hender, T. C., Carreras, B. A., Charlton, L. A. and Holmes J. A. 1987 *Phys. Fluids* **30**, 1756.

Hazeltine, R. D., Kotschenreuther, M. and Morrison P. J. 1985 *Phys. Fluids* **28**, 2466.

He, Z., Dong, J. Q., Long, Y. X., Mou, Z. Z., Gao, Z., He, H. D., Liu, F. and Shen, Y. 2010 *Phys. Plasmas* **17**, 112102.

Ishii, Y., Azumi, M. and Kishimoto, Y. 2002 *Phys. Rev. Lett.* **89**, 205002.

Ishii, Y., Azumi, M., Kurita, G. and Tuda, T. 2000 *Phys. Plasmas* **7**, 4477.

Ishii, Y., Smolyakov, A. I. and Takechi, M. 2009 *Nucl. Fusion* **49**, 085006.

Ishizawa, A., Sato, M. and Wakatani, M. 2003 *Phys. Plasmas* **10**, 3017.

Janvier, M., Kishimoto, Y. and Li, J. Q. 2011 *Phys. Rev. Lett.* **107**, 195001.

Kadomtsev, B. B. and Pogutse, O. P. 1967 *Sov. Phys. JETP* **24**, 1172.

Kaw, P. K., Valeo, E. J. and Rutherford, P. H. 1979 *Phys. Rev. Lett.* **43**, 1398.

Kleva, R. G., Drake, J. F. and Waelbroeck, F. L. 1995 *Phys. Plasmas* **2**, 23.

Matsumoto, T., Naitou, H., Tokuda, S. and Kishimoto, Y. 2005, *Nucl. Fusion* **45**, 1264.

Matsumoto, T., Tokuda, S., Kishimoto, Y., Takizuka, T. and Naitou, H. 1999 *J. Plasma Fusion Res.* **75**, 1188.

Nave, M. F. F. and Wesson, J. 1988 *Nucl. Fusion* **28**, 297.

https://doi.org/10.1017/S0022377812000554 Published online by Cambridge University Press

Ofman, L. 1992 *Phys. Fluids* B **4**, 2751.

Ofman, L., Chen, X. L., Morrison, P. J. and Steinolfson, R. S. 1991 *Phys. Fluids* B **3**, 1364.

Ottaviani, M. and Porcelli, F. 1993 *Phys. Rev. Lett.* **71**, 3802.

Ottaviani, M. and Porcelli, F. 1995 *Phys. Plasmas* **2**, 4104.

Papp, G., Pokol, G. I., Por, G., Magyarkuti, A., Lazányi, N., Horváth, L., Igochine, V., Maraschek, M. and ASDEX Upgrade Team 2011 *Plasma Phys. Control. Fusion* **53**, 065007.

Persson, M. 1991 *Nucl. Fusion* **31**, 382.

Persson, M. and Dewar, R. L. 1994 *Phys. Plasmas* **1**, 1256.

Porcelli, F. 1991 *Phys. Rev. Lett.* **66**, 425.

Pritchett, P. L., Lee, Y. C. and Drake, J. F. 1980 *Phys. Fluids* **23**, 1368.

Rosenbluth, M. N., Dagazian, R. Y. and Rutherford, P. H. 1973 *Phys. Fluids* **16**, 1894.

Rosenbluth, M. and Sloan, M. L. 1971 *Phys. Fluids* **14**, 1725.

Shen, C. and Liu, Z. X. 1998 *Plasma Phys. Control. Fusion* **40**, 1.

Strauss, H. R. 1976 *Phys. Fluids* **19**, 134.

Sun, Y., Wan, B., Hu, L., Chen, K., Shen, B. and Mao, J. 2009 *Plasma Phys. Control. Fusion* **51**, 065001.

Wang, X. and Bhattacharjee, A. 1993 *Phys. Rev. Lett.* **70**, 1627.

Wang, Z. X., Li, J., Dong, J. Q and Kishimoto, Y. 2009 *Phys. Rev. Lett.* **103**, 015004.

Wang, Z. X., Li, J., Dong, J. Q and Kishimoto, Y. 2011 *Phys. Plasmas* **18**, 012110.

Wang, Z. X., Li, J., Kishimoto, Y. and Dong, J. Q. 2009 *Phys. Plasmas* **16**, 060703.

Wang, Z. X., Wang, X. G., Dong, J. Q., Kishimoto, Y. and Li, J. Q. 2008 *Phys. Plasmas* **15**, 082109.

Wang, Z. X., Wang, X. G., Dong, J. Q., Lei, Y. A., Long, Y. X., Mou, Z .Z. and Qu, W. X. 2007 *Phys. Rev. Lett.* **99**, 185004.

Wang, Z. X., Wang, X. G., Dong, J. Q., Long, Y. X and Mou, Z. Z. 2007 *Plasma Science & Technology* **9**, 257.

Wang, X. Q., Wang, Z. X., Wei, L. and Xu, W. B. 2012 *Phys. Lett.* A **376**, 505.

Wang, X. Q., Wang, X., Xu, W. B. and Wang, Z. X. 2011a *Phys. Plasmas*, **18**, 012102.

Wang, Z. X., Wei, L., Wang, X. and Liu, Y. 2011b *Phys. Plasmas* **18**, 050701.

Wang, Z. X., Wei, L., Wang, X., Zheng, S. and Liu, Y. 2011c *Nucl. Fusion* **51**, 033003.

Wei, L. and Wang, Z. X. 2011 *Nucl. Fusion* **51**, 123005.

Wei, L., Wang, Z. X., Fan, D. M., Wang, F. and Liu, Y. 2011 *Phys. Plasmas* **18**, 042503.

Xu, X. Q., Dudson, B., Snyder, P. B., Umansky, M. V. and Wilson, H. 2010 *Phys. Rev. Lett.* **105**, 175005.

Yamada, M., Kulsrud, R. and Ji, H. 2010 *Rev. Mod. Phys.* **82**, 603–664.

Yu, Q. 1995 *Nucl. Fusion* **35**, 1012.

Yu, Q. and Günter, S. 1999 *Nucl. Fusion* **39**, 487.

Yuh, H. Y. Kaye, S. M., Levinton, F. M., Mazzucato, E., Mikkelsen, D. R., Smith, D. R., Bell, R. E., Hosea, J. C., LeBlanc, B. P., Peterson, J. L. et al. 2011 *Phys. Rev. Lett.* **106**, 055003.

Zhang, C. L. and Ma, Z. W. 2009 *Phys. Plasmas* **16**, 122113.

Zhao, X. M., Peng, X. D., Tang, C. J. and Qiu, X. M. 2011 *Phys. Plasmas* **18**, 072506.

https://doi.org/10.1017/S0022377812000554 Published online by Cambridge University Press